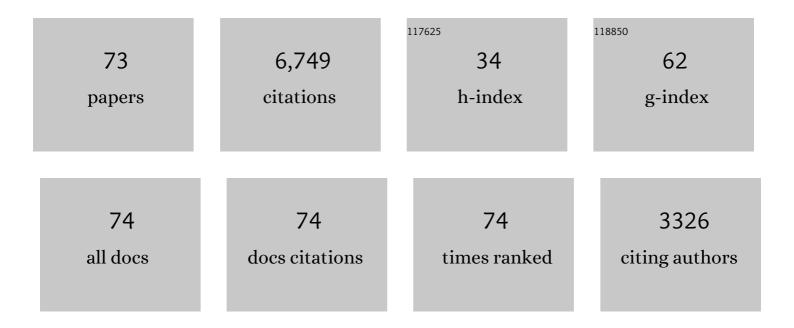
List of Publications by Year in descending order

Source: https://exaly.com/author-pdf/7369582/publications.pdf Version: 2024-02-01



F-C LIN

#	Article	IF	CITATIONS
1	3D Shear Wave Velocity Model of Salt Lake Valley via Rayleigh Wave Ellipticity across a Temporary Geophone Array. The Seismic Record, 2022, 2, 127-136.	3.1	Ο
2	Shallow Damage Zone Structure of the Wasatch Fault in Salt Lake City from Ambient-Noise Double Beamforming with a Temporary Linear Array. Seismological Research Letters, 2021, 92, 2453-2463.	1.9	4
3	Imaging the Subsurface Plumbing Complex of Steamboat Geyser and Cistern Spring With Hydrothermal Tremor Migration Using Seismic Interferometry. Journal of Geophysical Research: Solid Earth, 2021, 126, e2020JB021128.	3.4	13
4	Highâ€Resolution 3â€D Shear Wave Velocity Model of Northern Taiwan via Bayesian Joint Inversion of Rayleigh Wave Ellipticity and Phase Velocity With Formosa Array. Journal of Geophysical Research: Solid Earth, 2021, 126, e2020JB021610.	3.4	4
5	Shallow Crustal Shear Velocity and Vp/Vs Across Southern California: Joint Inversion of Shortâ€Period Rayleigh Wave Ellipticity, Phase Velocity, and Teleseismic Receiver Functions. Geophysical Research Letters, 2021, 48, e2021GL092626.	4.0	7
6	Analysis of Fault Zone Resonance Modes Recorded by a Dense Seismic Array Across the San Jacinto Fault Zone at Blackburn Saddle. Journal of Geophysical Research: Solid Earth, 2020, 125, e2020JB019756.	3.4	11
7	Shear Velocity Model of Alaska Via Joint Inversion of Rayleigh Wave Ellipticity, Phase Velocities, and Receiver Functions Across the Alaska Transportable Array. Journal of Geophysical Research: Solid Earth, 2020, 125, e2019JB018582.	3.4	41
8	Spatiotemporal Seismic Structure Variations Associated With the 2018 Kīlauea Eruption Based on Temporary Dense Geophone Arrays. Geophysical Research Letters, 2020, 47, e2019GL086668.	4.0	18
9	Eikonal Tomography of the Southern California Plate Boundary Region. Journal of Geophysical Research: Solid Earth, 2019, 124, 9755-9779.	3.4	28
10	High-resolution seismic tomography of Long Beach, CA using machine learning. Scientific Reports, 2019, 9, 14987.	3.3	27
11	Imaging the Deep Subsurface Plumbing of Old Faithful Geyser From Lowâ€Frequency Hydrothermal Tremor Migration. Geophysical Research Letters, 2019, 46, 7315-7322.	4.0	24
12	Structural Properties of the San Jacinto Fault Zone at Blackburn Saddle from Seismic Data of a Dense Linear Array. Pure and Applied Geophysics, 2019, 176, 1169-1191.	1.9	20
13	Ambient noise tomography across the Cascadia subduction zone using dense linear seismic arrays and double beamforming. Geophysical Journal International, 2019, 217, 1668-1680.	2.4	23
14	Low-Rank Matrix Completion for Distributed Ambient Noise Imaging Systems. , 2019, , .		1
15	Imaging the Fault Damage Zone of the San Jacinto Fault Near Anza With Ambient Noise Tomography Using a Dense Nodal Array. Geophysical Research Letters, 2019, 46, 12938-12948.	4.0	43
16	Real-Time Cooperative Analytics for Ambient Noise Tomography in Sensor Networks. IEEE Transactions on Signal and Information Processing Over Networks, 2019, 5, 375-389.	2.8	18
17	Wave equation dispersion inversion of surface waves recorded on irregular topography. Geophysical Journal International, 2019, 217, 346-360.	2.4	29
18	Imaging subsurface scatterers across a dense geophone array in Long Beach using noise crosscorrelation and natural inversion. , 2019, , .		0

#	Article	IF	CITATIONS
19	Rayleigh and S wave tomography constraints on subduction termination and lithospheric foundering in central California. Earth and Planetary Science Letters, 2018, 488, 14-26.	4.4	35
20	Upper Mantle Seismic Structure of Alaska From Rayleigh and <i>S</i> Wave Tomography. Geophysical Research Letters, 2018, 45, 10,350.	4.0	46
21	Seismically anisotropic magma reservoirs underlying silicic calderas. Geology, 2018, 46, 727-730.	4.4	51
22	Sequential Graph Scanning Statistic for Change-point Detection. , 2018, , .		9
23	Communication Efficient Signal Detection for Distributed Ambient Noise Imaging. , 2018, , .		2
24	Tomography of Southern California Via Bayesian Joint Inversion of Rayleigh Wave Ellipticity and Phase Velocity From Ambient Noise Crossâ€Correlations. Journal of Geophysical Research: Solid Earth, 2018, 123, 9933-9949.	3.4	40
25	Highâ€Resolution Receiver Function Imaging Across the Cascadia Subduction Zone Using a Dense Nodal Array. Geophysical Research Letters, 2018, 45, 12,218.	4.0	21
26	Lithospheric Structure Across the Alaskan Cordillera From the Joint Inversion of Surface Waves and Receiver Functions. Journal of Geophysical Research: Solid Earth, 2018, 123, 8780-8797.	3.4	30
27	Midcrustal Deformation in the Central Andes Constrained by Radial Anisotropy. Journal of Geophysical Research: Solid Earth, 2018, 123, 4798-4813.	3.4	33
28	Ambient noise tomography across Mount St. Helens using a dense seismic array. Journal of Geophysical Research: Solid Earth, 2017, 122, 4492-4508.	3.4	56
29	Real-Time Ambient Noise Subsurface Imaging in Distributed Sensor Networks. , 2017, , .		15
30	A one-dimensional seismic model for Uturuncu volcano, Bolivia, and its impact on full moment tensor inversions. , 2017, 13, 1-10.		47
31	Anatomy of Old Faithful From Subsurface Seismic Imaging of the Yellowstone Upper Geyser Basin. Geophysical Research Letters, 2017, 44, 10,240.	4.0	50
32	Wave-equation dispersion inversion of surface waves recorded on irregular topography. , 2017, , .		5
33	Amplification and Attenuation Across USArray Using Ambient Noise Wavefront Tracking. Journal of Geophysical Research: Solid Earth, 2017, 122, 10,086.	3.4	27
34	Offshore Rayleigh group velocity observations of the South Island, New Zealand, from ambient noise data. Geophysical Journal International, 2017, 209, 827-841.	2.4	5
35	Determination of Rayleigh wave ellipticity across the Earthscope Transportable Array using single-station and array-based processing of ambient seismic noise. Geophysical Journal International, 2017, 208, 234-245.	2.4	8
36	Lithospheric shear velocity structure of South Island, New Zealand, from amphibious Rayleigh wave tomography. Journal of Geophysical Research: Solid Earth, 2016, 121, 3686-3702.	3.4	14

#	Article	IF	CITATIONS
37	Imaging near-surface heterogeneities by natural migration of backscattered surface waves. Geophysical Journal International, 2016, 204, 1332-1341.	2.4	19
38	A seismic reference model for the crust and uppermost mantle beneath China from surface wave dispersion. Geophysical Journal International, 2016, 206, 954-979.	2.4	260
39	Highâ€resolution probing of inner core structure with seismic interferometry. Geophysical Research Letters, 2015, 42, 10,622.	4.0	27
40	The 11 March 2011 Tohoku tsunami wavefront mapping across offshore Southern California. Journal of Geophysical Research: Solid Earth, 2015, 120, 3350-3362.	3.4	8
41	Distinct crustal isostasy trends east and west of the Rocky Mountain Front. Geophysical Research Letters, 2015, 42, 10,290.	4.0	101
42	Site amplification, attenuation, and scattering from noise correlation amplitudes across a dense array in Long Beach, CA. Geophysical Research Letters, 2015, 42, 1360-1367.	4.0	51
43	The Yellowstone magmatic system from the mantle plume to the upper crust. Science, 2015, 348, 773-776.	12.6	220
44	3-D crustal structure of the western United States: application of Rayleigh-wave ellipticity extracted from noise cross-correlations. Geophysical Journal International, 2014, 198, 656-670.	2.4	98
45	A joint <scp>M</scp> onte <scp>C</scp> arlo analysis of seafloor compliance, <scp>R</scp> ayleigh wave dispersion and receiver functions at ocean bottom seismic stations offshore <scp>N</scp> ew <scp>Z</scp> ealand. Geochemistry, Geophysics, Geosystems, 2014, 15, 5051-5068.	2.5	24
46	<i>P</i> and <i>S</i> wave tomography of the mantle beneath the United States. Geophysical Research Letters, 2014, 41, 6342-6349.	4.0	198
47	Upper crustal azimuthal anisotropy across the contiguous U.S. determined by Rayleigh wave ellipticity. Geophysical Research Letters, 2014, 41, 8301-8307.	4.0	36
48	Ambient noise crossâ€correlation observations of fundamental and higherâ€mode Rayleigh wave propagation governed by basement resonance. Geophysical Research Letters, 2013, 40, 3556-3561.	4.0	42
49	Seismic interferometry with antipodal station pairs. Geophysical Research Letters, 2013, 40, 4609-4613.	4.0	51
50	Extracting seismic core phases with array interferometry. Geophysical Research Letters, 2013, 40, 1049-1053.	4.0	99
51	High-resolution 3D shallow crustal structure in Long Beach, California: Application of ambient noise tomography on a dense seismic array. Geophysics, 2013, 78, Q45-Q56.	2.6	333
52	Joint inversion of surface wave dispersion and receiver functions: a Bayesian Monte-Carlo approach. Geophysical Journal International, 2013, 192, 807-836.	2.4	202
53	Ambient seismic noise tomography of Canada and adjacent regions: Part I. Crustal structures. Journal of Geophysical Research: Solid Earth, 2013, 118, 5865-5887.	3.4	50
54	Joint inversion of Rayleigh wave phase velocity and ellipticity using USArray: Constraining velocity and density structure in the upper crust. Geophysical Research Letters, 2012, 39, .	4.0	95

#	Article	IF	CITATIONS
55	The local amplification of surface waves: A new observable to constrain elastic velocities, density, and anelastic attenuation. Journal of Geophysical Research, 2012, 117, .	3.3	52
56	Interferometry with a dense 3D dataset. , 2012, , .		0
57	On the reliability of attenuation measurements from ambient noise cross-correlations. Geophysical Research Letters, 2011, 38, n/a-n/a.	4.0	33
58	Ambient noise tomography with a large seismic array. Comptes Rendus - Geoscience, 2011, 343, 558-570.	1.2	105
59	Helmholtz surface wave tomography for isotropic and azimuthally anisotropic structure. Geophysical Journal International, 2011, 186, 1104-1120.	2.4	158
60	Apparent anisotropy in inhomogeneous isotropic media. Geophysical Journal International, 2011, 186, 1205-1219.	2.4	16
61	Complex and variable crustal and uppermost mantle seismic anisotropy in the western UnitedÂStates. Nature Geoscience, 2011, 4, 55-61.	12.9	151
62	Seismic evidence for widespread western-US deep-crustal deformation caused by extension. Nature, 2010, 464, 885-889.	27.8	178
63	Crustal shear wave velocity structure of the western United States inferred from ambient seismic noise and earthquake data. Journal of Geophysical Research, 2010, 115, .	3.3	94
64	Eikonal tomography: surface wave tomography by phase front tracking across a regional broad-band seismic array. Geophysical Journal International, 2009, 177, 1091-1110.	2.4	326
65	Surface wave tomography of the western United States from ambient seismic noise: Rayleigh and Love wave phase velocity maps. Geophysical Journal International, 2008, 173, 281-298.	2.4	634
66	Structure of the crust and uppermost mantle beneath the western United States revealed by ambient noise and earthquake tomography. Journal of Geophysical Research, 2008, 113, .	3.3	175
67	Processing seismic ambient noise data to obtain reliable broad-band surface wave dispersion measurements. Geophysical Journal International, 2007, 169, 1239-1260.	2.4	1,705
68	Ambient noise Rayleigh wave tomography of New Zealand. Geophysical Journal International, 2007, 170, 649-666.	2.4	255
69	Is ambient noise tomography across ocean basins possible?. Geophysical Research Letters, 2006, 33, .	4.0	32
70	Temperature control device for single molecule measurements using the atomic force microscope. Review of Scientific Instruments, 2006, 77, 063701.	1.3	10
71	Reversible Mechanical Unfolding of Single Ubiquitin Molecules. Biophysical Journal, 2004, 87, 3995-4006.	0.5	87
72	Empirically determined finite frequency sensitivity kernels for surface waves. Geophysical Journal International, 0, 182, 923-932.	2.4	16

	С		
_	1 a c		N
	<u> </u>	-	

#	Article	IF	CITATIONS
73	Isolating and Tracking Noise Sources across an Active Longwall Mine Using Seismic Interferometry. Bulletin of the Seismological Society of America, 0, , .	2.3	2